Journal of Power Sources 195 (2010) 6680–6687

Contents lists available at ScienceDirect

Journal of Power Sources

journal homepage: www.elsevier.com/locate/jpowsour

Water transport during startup and shutdown of polymer electrolyte fuel cell stacks

X. Wang, K. Tajiri, R.K. Ahluwalia*

Argonne National Laboratory, 9700 S Cass Avenue, Argonne, IL 60439, USA

ARTICLE INFO

Article history:
Received 20 February 2010
Received in revised form 2 April 2010
Accepted 5 April 2010
Available online 10 April 2010

Keywords:
Polymer electrolyte fuel cells
Cold-start
Shutdown

ABSTRACT

A dynamic three-phase transport model is developed to analyze water uptake and transport in the membrane and catalyst layers of polymer electrolyte fuel cells during startup from subfreezing temperatures and subsequent shutdown. The initial membrane water content (λ, the number of water molecules per sulfonic acid site) is found to be an important parameter that determines whether a successful unassisted self-start is possible. For a given initial subfreezing temperature at startup, there is a critical λ (λ_h), above which self-start is not possible because the product water completely engulfs the catalyst layers with ice before the stack can warm-up to 0 °C. There is a second value of λ (λ_l), below which the stack can be self-started without forming ice. Between λ_l and λ_h, the stack can be self-started, but with intermediate formation of ice that melts as the stack warms up to 0 °C. Both λ_l and λ_h are functions of the initial stack temperature, cell voltage at startup, membrane thickness, catalyst loading, and stack heat capacity. If the stack is purged during the previous shutdown by flowing air in the cathode passages, then depending on the initial amount of water in the membrane and gas diffusion layers and the initial stack temperature, it may not be possible to dry the membrane to the critical λ for a subsequent successful startup. There is an optimum λ for robust and rapid startup and shutdown. Startup and shutdown time and energy may be unacceptable if the λ is much less than the optimum. Conversely, a robust startup from subfreezing temperatures cannot be assured if the λ is much higher than this optimum.

1. Introduction

Polymer electrolyte fuel cells (PEFC) for transportation must be able to start unassisted from temperatures below −20 °C and produce 50% of their rated power within 30 s while using less than 5 MJ of fuel energy for startup and shutdown of an 80-kWe system [1]. At subfreezing temperatures, the water produced by the electrochemical reaction coats the cathode catalyst with ice that reduces the effective electrochemically active surface area (ECSA) and may terminate the reaction. It may be possible to prevent ice formation by operating at low current densities and using dry gas feeds at high flow rates, but these operating conditions lead to unacceptable startup times and energies. Fast start may involve the formation of ice and presents the challenge to effectively manage the buildup of ice [2]. A proper understanding of water transport during startup (and the previous shutdown) is essential to determining the conditions under which the stack can be started rapidly from subfreezing temperatures, even if some ice may be formed initially at startup.

Isothermal behavior of single cells at subfreezing temperatures has been reported in a number of investigations. Hishinuma et al. [3] monitored voltage decay at constant current of a 104-cm^2 cell placed inside a climate-controlled chamber at −10 to −25 °C. They concluded that a cell could not be started from temperatures below −5 °C without external heating. Oszipok et al. [4] extended this study to include the effect of initial membrane water content on isothermal potentiostatic behavior of a single cell. They inferred from their experimental data that initial membrane drying is beneficial in successful self-start from −20 °C, but that the membrane should not be too dry. Tajiri et al. [5] confirmed the beneficial effect of initial membrane drying and also investigated the effects of initial gas purge and membrane thickness on cold-start behavior. In follow-up papers, Ge and Wang [6,7] reported observations from visualizations of ice formation and cyclic voltammetry data on the effect of ice coverage on the oxygen reduction kinetics. Pinton et al. [8] conducted isothermal and galvanostatic tests to study cold-start behavior as a function of various operating parameters, including initial water content, cell voltage and current density. They observed an optimal wetting level that maximizes the heat generated from the electrochemical reaction.

* Corresponding author at: Argonne National Laboratory, Nuclear Engineering Division, 9700 S Cass Avenue, Argonne, IL 60439, USA. Tel.: +1 630 252 5979; fax: +1 630 252 5287.
E-mail address: walia@anl.gov (R.K. Ahluwalia).

0378-7753/$ – see front matter © 2010 Elsevier B.V. All rights reserved.
doi:10.1016/j.jpowsour.2010.04.012

Nomenclature

A	specific area
a	activity
D	diffusivity
F	Faraday constant
h	mass transfer coefficient
I	current density
$\dot{I}$	volumetric reaction rate
J	Leverett function
K	absolute permeability
k_r	relative permeability
S	water saturation level
t	time
u	velocity
y	transverse direction
β	osmotic drag coefficient
δ	step function
ε	volume fraction
κ	ionic conductivity
λ	membrane water content
μ	viscosity
ρ	molar density
ρ_m	membrane density divided by equivalent weight
σ	surface tension

Subscripts/superscripts

eff	effective
H^+	proton
h	upper limit
i	ice, initial
l	liquid water, lower limit
m	membrane, ionomer
max	maximum
ORR	oxygen reduction reaction
s	saturation
v	vapor

There are only limited experimental and theoretical studies on non-isothermal startup from subfreezing temperatures. Ahluwalia and Wang [2] investigated the conditions for rapid start including the effect of cell voltage and heat capacity of stack materials. Conti [9] reports experimental data on time and energy consumed in cold-start of a short stack. Other manufacturers [10–12] have also reported successful startup from temperatures down to −30 °C. Multi-dimensional models of cold-start have also started to appear in the open literature [13,14].

Water removal from fuel cells by gas purging during shutdown is a subject of current interest. Sinha and Wang [15] formulated a simple model to characterize water transport across the membrane and gas diffusion layers in purge drying. Tajiri et al. [16] presented some initial data on the drying process using high-frequency resistance of the cell as an indicator of the water content. Owejan et al. [17] examined water transport in fuel cells by using in situ and ex situ methods and used the data to formulate a one-dimensional model for calculating the effectiveness of cathode purge for removing water from fuel cells at shutdown.

Many publications have recently appeared on the fundamental properties of membranes and electrocatalytic activity at subfreezing temperatures. Thompson et al. [18] have investigated low temperature proton transport in Nafion using direct current four-point probe for conductivity measurements and differential scanning calorimetry for melting and freezing of membrane water. In subsequent work, Thompson et al. [19–21] developed an experimental procedure to measure oxygen reduction reaction kinetics at subfreezing temperatures and investigated ice formation, water (charge) storage, current distribution, and voltage losses during isothermal cold-start. Gallagher et al. [22] measured electro-osmosis and water uptake in polymer electrolytes in equilibrium with water vapor at low temperatures. References [2,18–22] may be consulted for other literature on membrane properties and electrocatalyst activities at low temperatures.

Table 1
Stack parameters.

Stack gross power	93.5 kW
Stack weight	56 kg
Number of cells	452
Cell voltage at rated power	663 mV
Platinum loading (*a*/*c*)	0.1/0.2 mg cm^{-2}
Active area per cell	329 cm^2
Active area to total area	85%
Graphite bipolar plate thickness	200 μm
Gas channel depth/width	0.5/3 mm
Land shoulder width	0.6 mm
GDL thickness	260 μm
GDL porosity, ε	60%
GDL gas permeability, K	2.55×10^{-13} m^2
GDL contact angle	100°
Catalyst layer thickness (*a*/*c*)	4/6 μm
Catalyst layer porosity, ε	46%
Ionomer volume fraction, ε_m	23%
Membrane thickness	25 μm
Bulk density of ice	500 kg m^{-3}

In this work, we investigate the effect of water transport on startup and shutdown at subfreezing temperatures. It builds on the earlier work reported in Ref. [2] and provides a theoretical underpinning for the experimental observations concerning the effect of initial water content on startup from cold [4,5,8]. It also reports theoretical purge drying of stacks to prepare membrane electrode assemblies for subsequent successful startup from cold temperatures.

2. Water transport model

We have formulated a model to determine water transport during startup and shutdown. The model tracks water transport across the membrane and the ionomer in the catalyst layers in terms of λ, the number of water molecules per sulfonic acid site, by solving a set of transient equations that consider diffusion and electro-osmotic drag. Eq. (1) describes water transport across the solid membrane.

$$\frac{\partial}{\partial t}(\rho_m \lambda) = \frac{\partial}{\partial y}\left(\rho_m D_\lambda^{eff}\frac{\partial \lambda}{\partial y} - \beta_\lambda \frac{I_{H^+}}{F}\right) \quad (1)$$

During startup from subfreezing temperatures, water can be present in the catalyst layers in three phases: solid ionomer, interstitial vapor and ice. The following conservation equations describe the movement of water within the ionomer (subscript *m*), vapor (subscript *v*) and ice (subscript *i*) phases by various mechanisms, including interfacial mass transfer.

$$\frac{\partial}{\partial t}(\rho_m \varepsilon_m \lambda) = \frac{\partial}{\partial y}\left(\rho_m \varepsilon_m D_\lambda^{eff}\frac{\partial \lambda}{\partial y} - \beta_\lambda \frac{I_{H^+}}{F}\right) + \frac{\dot{I}_{ORR}}{2F} - h_m A_m(\rho_{mv} - \rho_v) \quad (2)$$

$$\frac{\partial}{\partial t}(\varepsilon \rho_v) = \frac{\partial}{\partial y}\left(D_v^{eff}\frac{\partial \rho_v}{\partial y}\right) + h_m A_m(\rho_{mv} - \rho_v) - h_c A_c(\rho_v - \rho_s) \quad (3)$$

$$\frac{\partial}{\partial t}(\rho_i \varepsilon S) = h_c A_c(\rho_v - \rho_s) \tag{4}$$

We assume that because of large mass transfer coefficients and/or large specific areas, water is in equilibrium among the three phases, so that water uptake in the ionomer can be expressed in terms of the water saturation level (S) by the well-known relationships,

$$\lambda = \lambda_s + (\lambda_{\max} - \lambda_s)S, \quad \lambda > \lambda_s \tag{5}$$

$$\lambda = 0.043 + 17.81a - 39.85a^2 + 36a^3 \quad , \lambda < \lambda_s \tag{6}$$

where a is the activity of water vapor,

$$a = \frac{\rho_v}{\rho_s} \tag{7}$$

and for Nafion at 80 °C,

$$\lambda_s = 14 \text{ and } \lambda_{\max} = 16.8 \tag{8}$$

With the assumption of phase equilibrium, Eqs. (2)–(4) may be combined into a single equation for water transport:

$$\frac{\partial}{\partial t}\left(\rho_m \varepsilon_m \lambda + \varepsilon \rho_s a(\lambda) + \rho_i \varepsilon \frac{\lambda - \lambda_s}{\lambda_{\max} - \lambda_s}\delta\right) = \frac{\partial}{\partial y}\left(\left(\rho_m \varepsilon_m D_\lambda^{eff} + \rho_s(1-\delta)D_v^{eff}\frac{\partial a}{\partial \lambda}\right)\frac{\partial \lambda}{\partial y} - \beta_\lambda \frac{I_{H^+}}{F}\right) + \frac{\dot{I}_{ORR}}{2F} \tag{9}$$

where δ is a step function, defined as:

$$\delta = \begin{cases} 1 & \lambda > \lambda_s \\ 0 & \lambda \le \lambda_s \end{cases} \tag{10}$$

and we have used the following chain rule,

$$\frac{\partial \rho_v}{\partial y} = \rho_s \frac{\partial a}{\partial y} = \rho_s \frac{\partial a}{\partial \lambda}\frac{\partial \lambda}{\partial y} \tag{11}$$

During startup from above-freezing temperatures and during shutdown, water may be present as a liquid that is not stationary. In this case, Eq. (4) modifies to Eq. (12) that considers capillary movement of water,

$$\frac{\partial}{\partial t}(\rho_l \varepsilon S) + \frac{\partial}{\partial y}(\rho_l u_l) = h_c A_c(\rho_v - \rho_s) \tag{12}$$

Without loss of generality, we assume that the liquid velocity can be represented by a Leverett type of $J(S)$ function,

$$u_l = \frac{\sigma \cos\theta_c}{\mu_l}(\varepsilon K)^{1/2} k_r \frac{dJ(S)}{dS}\frac{dS}{dy} \tag{13}$$

We add Eqs. (2), (3) and (12) to eliminate the interfacial mass transfer terms, invoke the assumption of phase equilibrium, and arrive at the following single equation for water transport across the catalyst layers.

$$\frac{\partial}{\partial t}\left(\rho_m \varepsilon_m \lambda + \varepsilon \rho_s a(\lambda) + \rho_l \varepsilon \frac{\lambda - \lambda_s}{\lambda_{\max} - \lambda_s}\delta\right) = \frac{\partial}{\partial y}\left(\left(\rho_m \varepsilon_m D_\lambda^{eff} + \rho_s(1-\delta)D_v^{eff}\frac{\partial a}{\partial \lambda} + \delta D_l\right)\frac{\partial \lambda}{\partial y} - \beta_\lambda \frac{I_{H^+}}{F}\right) + \frac{\dot{I}_{ORR}}{2F} \tag{14}$$

In the above equation, D_l may be regarded as diffusivity of liquid water due to capillary movement,

$$D_l = -\rho_l \frac{\sigma \cos\theta_c}{\mu_l}(\varepsilon K)^{1/2} k_r \frac{dJ(S)}{dS}\frac{dS}{d\lambda} \tag{15}$$

At subfreezing temperatures, the state of water may be classified as freezing (free water), bound freezable, and bound non-freezable [23]. In our model, λ refers to the total water content in the membrane and ionomer, without explicitly distinguishing between the states of water. The transport properties (D_λ^{eff} and β_λ), however, implicitly depend on the state of water.

Eq. (14) may be regarded as a single equation that describes three-phase transport of water in the catalyst layers at all temperatures, if one considers D_l to be zero at subfreezing temperatures. It considers parallel movement of water by diffusion in the ionomer due to activity gradient, vapor diffusion in the voids, capillary movement of liquid, and electro-osmotic drag. If the assumption of phase equilibrium applies, Eq. (14) can be solved to determine the formation and possible melting of ice during startup from subfreezing temperatures and removal of water during purge at shutdown. Note that Eq. (14) is equally applicable to anode (ACL) and cathode catalyst layers (CCL) by taking $\dot{I}_{ORR}$ to equal zero in the ACL.

The complete water transport model solves Eq. (1) for the λ profile in the membrane, Eq. (14) for λ, activity and S profiles in the catalyst layers, and additional equations that describe capillary movement in the anode and cathodes gas diffusion layers. We have developed a special analytical procedure to monitor the location and movement of the liquid interface within the GDLs during purge at shutdown.

As pointed out in Ref. [2], ice can also form in the GDL. The fraction of the water formed by ORR that appears as ice in the GDL depends on the water formation rate (i.e., current density), the rate at which water diffuses from the CCL to the GDL, and vapor condensation kinetics. We are in the process of formulating a model to calculate the temperature profile across the MEA and determine thermal gradient driven water diffusion (and ice formation) into the GDL.

For brevity and because they are documented elsewhere [2], we do not list the energy, species and electrochemical equations that need to be solved simultaneously with the water transport equations.

3. Model validation

We have calibrated the water transport model with the isothermal single cell data reported by Tajiri et al. [5]. We analyzed the high-frequency resistance (HFR) data since the change in HFR is a measure of the dynamics of water uptake in the membrane and the ionomer in the catalyst layers. We derived the following correlations from the independent experimental data for water uptake and conductivity of the Gore membrane used in the experimental setup.

$$\lambda = 20.5a^4 - 20.9a^3 + 2.61a^2 + 7.58a - 0.0985$$
$$\kappa = \left(3.2 \times 10^{-3}\lambda - 2.0 \times 10^{-3}\right)\exp\left[2222\left(\frac{1}{303} - \frac{1}{T}\right)\right] \tag{16}$$

According to the results of our analysis, the membrane dries out at −30 °C if we use 20 kJ mol^{-1} activation energy in the expression for water diffusivity in the membrane (D_λ^{eff}) and unity electro-osmotic drag coefficient (β_λ). The model can explain the HFR data only if the activation energy for D_λ^{eff} and/or β_λ are lower. Fig. 1 shows the comparison between the HFR data and the model results obtained by scaling down β_λ to 0.1 at −30 °C. One reason that the effective β_λ can be lower at subfreezing temperatures is that only a fraction of the membrane water is mobile, assuming that the fraction that is frozen cannot move. However, less than 50% of the membrane water is expected to freeze at −30 °C [18].

4. Results and discussion

We have used our model to conduct a parametric study of PEMFC stack startup and shutdown as a function of the initial water content, stack temperature and ambient temperature. For the purpose of this study, the stack is assumed to have dispersed

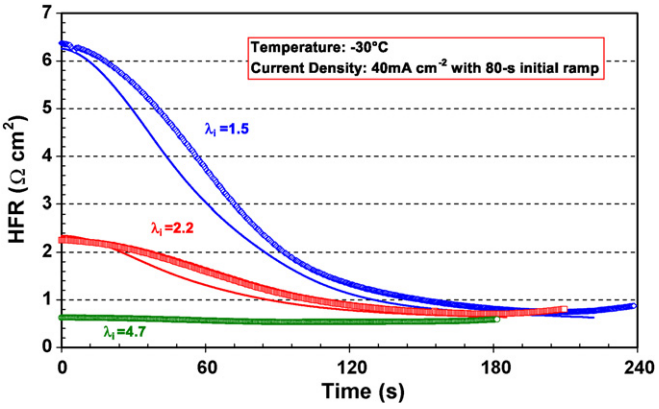

Fig. 1. Effect of λ_i on cell high-frequency resistance in isothermal tests.

Pt/C catalysts with 0.1(a)/0.2(c) mg cm^{-2} Pt loading, 25-μm Nafion membrane (N111), 200-μm thick gas diffusion layers (GDLs) with 60-μm thick microporous layers (MPLs), graphite bipolar plates, and 1680 W kg^{-1} specific power corresponding to 663-mV cell voltage at rated power (see Table 1). Ref. [2] may be consulted for the parameters that characterize the electrochemical oxidation reaction on the anode catalyst and the oxygen reduction reaction (ORR) on the cathode catalyst. In our study, we used the following correlation for proton conductivity (S cm^{-1}) at subfreezing temperature (T < 273 K, λ > 1), which was derived from the four-point probe data of Thompson et al [18].

$$\frac{E}{R} = -32.025\lambda^3 + 619.76\lambda^2 - 3770.2\lambda + 10722$$
$$\kappa = \left(-4.2263 \times 10^{-5}\lambda^2 + 1.2631 \times 10^{-3}\lambda - 0.0023\right) \exp\left(\frac{E}{R}\left(\frac{1}{243} - \frac{1}{T}\right)\right) \quad (17)$$

Many factors, in addition to those investigated in this study, influence the startup behavior of large stacks from subfreezing temperatures. These include cell-to-cell variations in temperature, especially in the cells near the bulky end plates that will warm-up slowly, cell voltage variation due to gas maldistribution caused by ice blockage, and variable contact resistance due to non-uniform compression of large-area cells.

4.1. Startup from subfreezing temperatures

We have determined the conditions under which PEFC stacks can be self-started rapidly from subfreezing temperatures. Fig. 2 presents selected results from simulations for startup from −20 °C at constant cell voltage (0.6 V) and ambient pressure. It shows that the initial water content of the membrane is an important parameter that determines whether a successful unassisted self-start is possible. There is a critical λ_i (λ_h = 8 for the conditions of Fig. 2) above which self-start is not possible because the product water completely engulfs the catalyst with ice before the stack can warm-up to 0 °C. There is a second value of λ_i (λ_l = 5 for the conditions of Fig. 2), below which the stack can be self-started without forming ice. Between λ_l and λ_h (see results for λ_i = 7.5), the stack can be self-started but with the intermediate formation of ice that melts as the stack warms up to 0 °C.

Our simulations show that the startup from a subfreezing temperature is robust for $\lambda_i < \lambda_l$, since the membrane absorbs sufficient amount of product water that ice does not form during the time that the stack warms up to 0 °C. Startup under this condition results in the current density monotonically increasing with time. During startup for $\lambda_l < \lambda_i < \lambda_h$ (see results for λ_i = 7.5), product water is initially absorbed in the membrane until it becomes locally saturated (λ_s = 14 for Nafion, 1100 equivalent weight) after which ice begins to form. Startup for $\lambda_l < \lambda_i < \lambda_h$ results in the current density initially increasing with time because of the improvement in membrane proton conductivity and the catalyst activity due to water uptake and temperature rise, and then decreasing with time because of the reduction in ECSA due to ice formation. With an initial λ greater than 14, all of the product water turns into ice, and the current density decreases monotonically with time.

Both λ_l and λ_h are functions of the initial stack temperature and the cell voltage at startup. The higher the initial stack temperature and the lower the startup cell voltage, the higher are λ_l and λ_h. These critical λ_i values are also functions of the membrane thickness, catalyst loading (volume of voids in catalyst layers), and stack specific power (effective heat capacity).

Fig. 2 shows that the rise in stack temperature mirrors the variation in the current density. The rate at which the stack temperature rises is relatively high during the time of increasing current density (i.e., production of waste heat) and it then decreases as the current density declines because of ice formation. The inflection points in the curves of current density vs. time and the rate of temperature rise vs. time denote the onset of ice formation. The stack temperature asymptotically approaches a value less than 0 °C if the initial $\lambda_i > \lambda_h$, resulting in a failure to start.

Fig. 3 shows that, similar to critical λ_i, there is a maximum cell voltage (V_c) for self-start that is a function of the initial temperature and λ, $V_c = V_c(T_i, \lambda_i)$. For example, self-start is not possible from −20 °C and λ_i = 7.5 for V_{cell} > 0.7. At these initial conditions, the cell can be self-started at 0.6 V cell voltage, although ice forms at intermediate times prior to the stack warming to 0 °C. Fig. 3 indicates that the self-start occurs without ice formation at 0.5 V cell voltage. Also, the lower the cell voltage, the more the production of waste

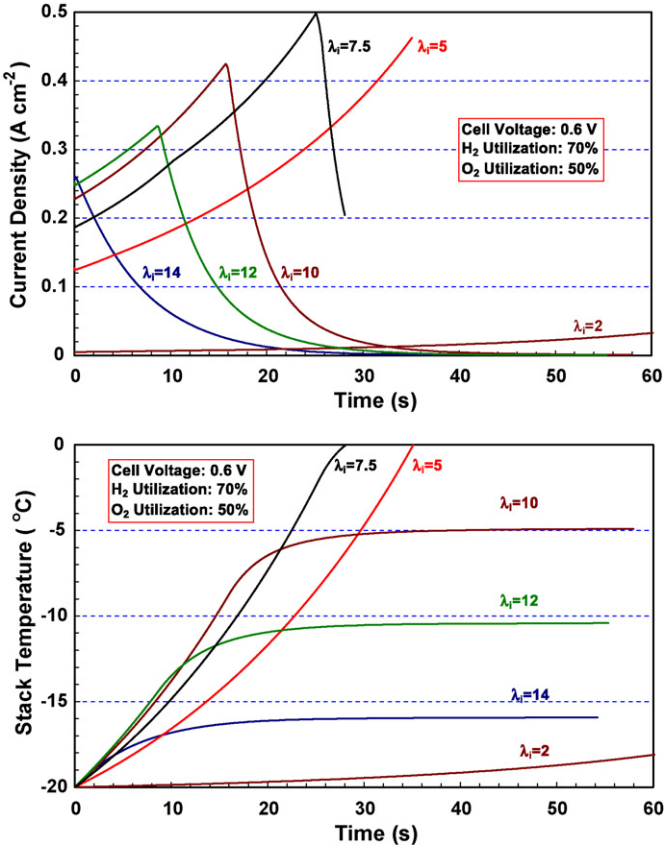

Fig. 2. Effect of λ_i on current density and stack temperature during startup from −20 °C at 0.6 V.

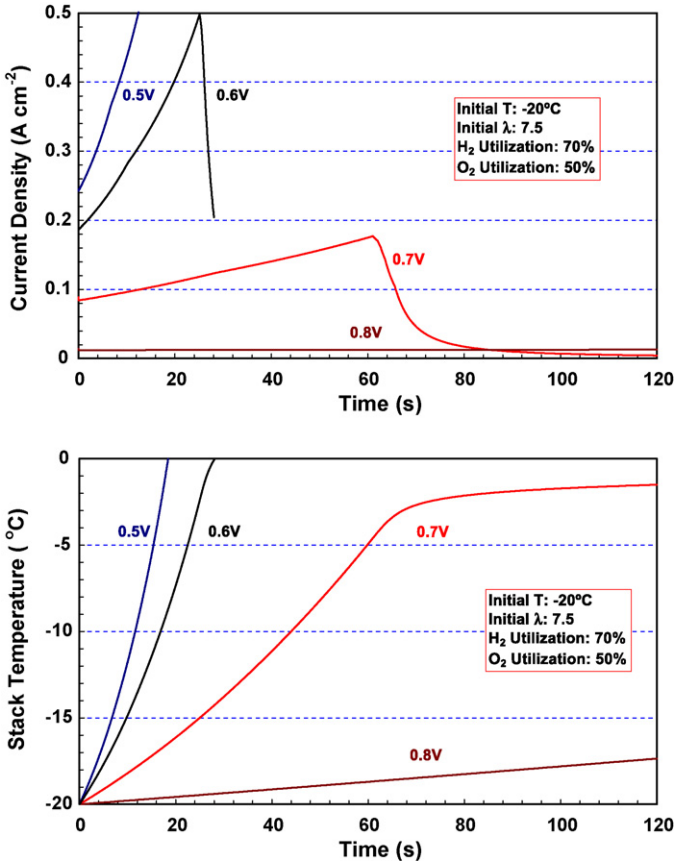

Fig. 3. Effect of cell voltage on current density and stack temperature during startup from −20 °C, λ_i = 7.5.

heat, and the faster is the startup. As expected, the results from simulations not shown here confirm that V_c increases with increase in T_i and with decrease in λ_i.

Similar to critical λ_i and cell voltage, there is a critical temperature for self-start that is a function of the cell voltage and initial λ, $T_c = T_c(V_{cell}, \lambda_i)$ For example, Fig. 4 shows that whereas the stack can be self-started from −20 °C with intermediate ice formation, and from −10 °C without forming ice at λ_i = 7.5 and V_{cell} = 0.6 V, self-start is not possible under these conditions for T_i lower than −30 °C. However, simulations indicate that self-start is possible from −30 °C at lower V_{cell} and λ_i.

Fig. 5 presents the time it takes to warm the stack to 0 °C for different initial temperatures, λ_i, and V_{cell}. The minimum warm-up time generally corresponds to the lowest cell voltage and λ_i close to λ_h, at which condition ice is formed during intermediate time. At very low initial temperatures (see results for −30 °C), there is a high propensity to form ice that impedes the ORR reaction so that the minimum in warm-up time occurs at $\lambda_i < \lambda_h$. The startup is more robust (no ice formation) if $\lambda_i < \lambda_l$ but the warm-up time generally increases with a decrease in λ_i. As seen in Fig. 2, the startup time can be much longer than 60 s for λ_i = 2 and −20 °C initial temperature. For $\lambda_i < \lambda_l$, lowering λ_i causes the current density to decrease because of reduction in the electrical conductivity. This, in turn, slows the production of waste heat and hence stretches the warm-up period.

4.2. Stack shutdown

We ran simulations to determine the time and energy required to dry the membrane to the λ at which a subsequent self-start is possible. We assumed that only the cathode is purged with ambient air and that the anode side is isolated. Fig. 6 presents the time and spatial variation of the membrane water content for a simulation with 50 °C initial stack temperature, 0.2 saturation (i.e., 20% of the volume of pores and void space filled with liquid water) of cathode GDL and CCL, and 0.04 saturation of anode GDL and ACL. The temporal λ profiles exhibit two inflexion points, the first of which marks the complete removal of liquid water from the cathode GDL/CCL and the onset of removal of liquid water from the anode GDL/ACL. The second inflexion point denotes the complete removal of liquid water from the anode GDL/CCL and the onset of membrane dehydration. Fig. 6 indicates that, because of the greater transport distance with the cathode-only purge, it takes longer to remove liquid water from the anode GDL/ACL even though the cathode GDL holds more water. Similarly, depending on the target λ, membrane dehydration takes a long time because the effective diffusivity of water in the membrane is relatively low and it decreases sharply as λ drops below about 3.

Fig. 6 indicates that depending on the initial conditions and the purge time, the λ profile can be non-uniform. In addition, it may not be practical to dehydrate the membrane to a very low λ value near the stack outlet. In all following discussions, target λ refers to the desired λ averaged over the membrane thickness and length after the purge period.

Fig. 7 shows the calculated variation in purge time with initial stack temperature and water content, and target λ, assuming that the flow rate is adjusted to maintain 30% relative humidity at stack exit. Given the target λ and saturation levels, the required purge (shutdown) time increases with decrease in the initial stack temperature. The results in Fig. 7 indicate that it may not be feasible to purge the stack to reach a target λ if the stack temperature at shutdown is below a minimum temperature. The lower the target λ or the higher the saturation levels, the higher is the minimum

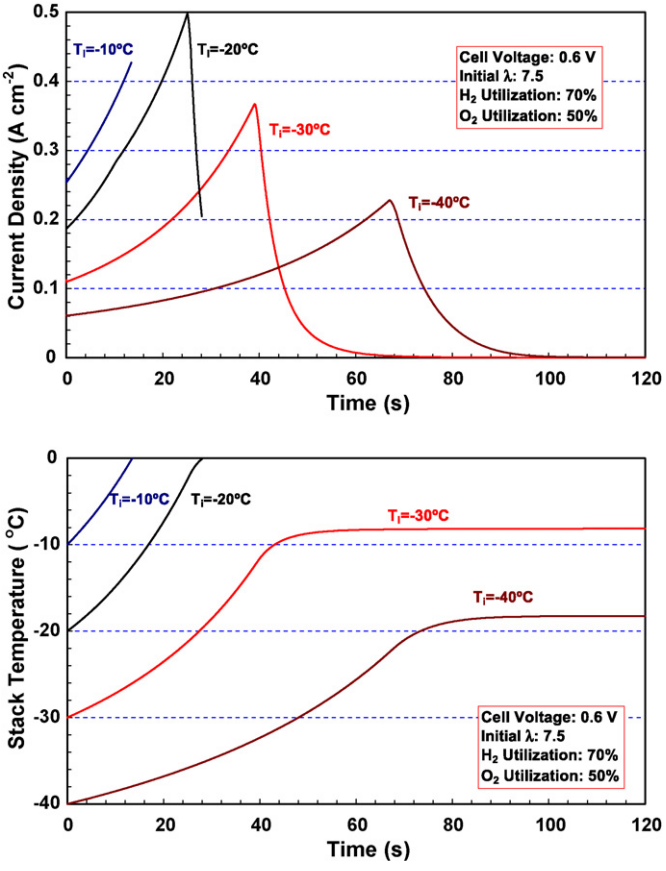

Fig. 4. Effect of initial stack temperature on startup at 0.6 V, λ_i = 7.5.

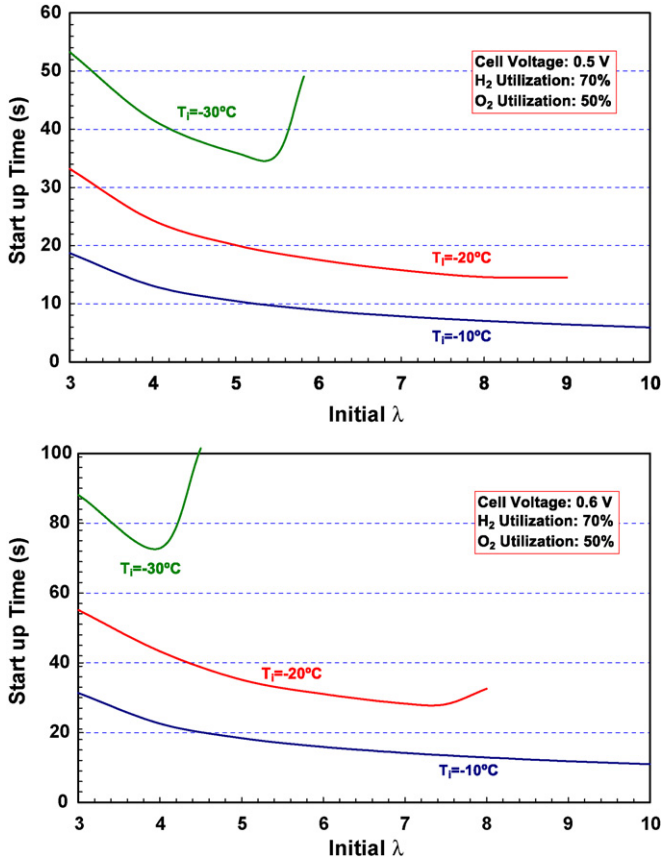

Fig. 5. Time to warm-up to 0 °C for different λ_i, cell voltages and initial temperatures.

initial temperature. For example, for the conditions of Fig. 7, the stack cannot be purged to reach a target λ of 9 if the initial stack temperature is below 35 °C and the cathode/anode saturations are 0.1/0.02. This minimum temperature increases to about 42 °C if the initial cathode/anode saturations are higher (S_C/S_A = 0.2/0.04) and further increases to about 50 °C if the target λ is also lower (target λ = 4). These results point to a potential problem of shutdown failure (inability to reach target λ) if a fuel cell vehicle is parked after a short drive on a cold day before the stack reaches its normal operating temperature. This problem can be overcome (at the expense of energy efficiency) by not allowing the stack to shutdown until it has reached the minimum temperature.

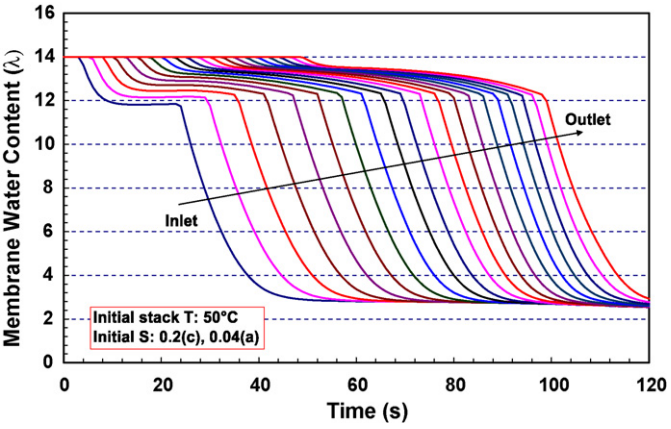

Fig. 6. Drying of membrane with purging of cathode with air (no anode purge).

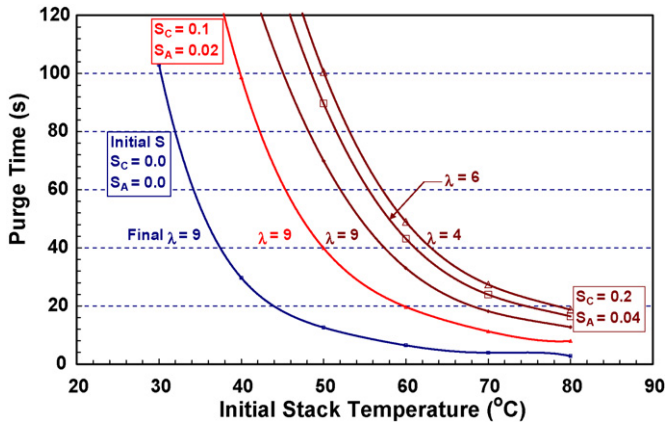

Fig. 7. Purge time as a function of initial saturation, stack temperature and target λ.

Fig. 8 presents the stack temperature profiles during shutdown under two sets of conditions, one for which the target λ can be reached (top plot) and the other for which the target λ cannot be reached (bottom plot). It shows that the cooling front initially marches along the flow direction (i.e., from stack inlet to stack outlet) and that the stack temperature can drop below the inlet gas temperature because of the latent heat of vaporization. After a certain period, the temperature profile can reverse once the front portion of the stack rewarms to the gas inlet temperature while the back portion is still drying out.

Besides initial stack temperature and saturation levels and target λ, the required purge time also depends on the ambient temperature and the stack heat capacity. The higher the ambient temperature or the stack heat capacity, the shorter is the purge

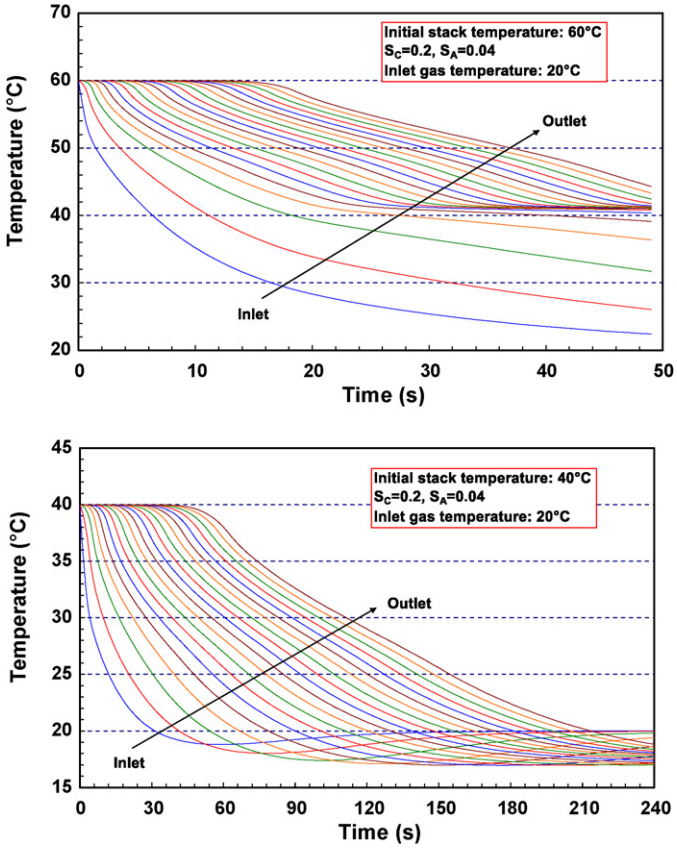

Fig. 8. Stack temperature profiles during shutdown.

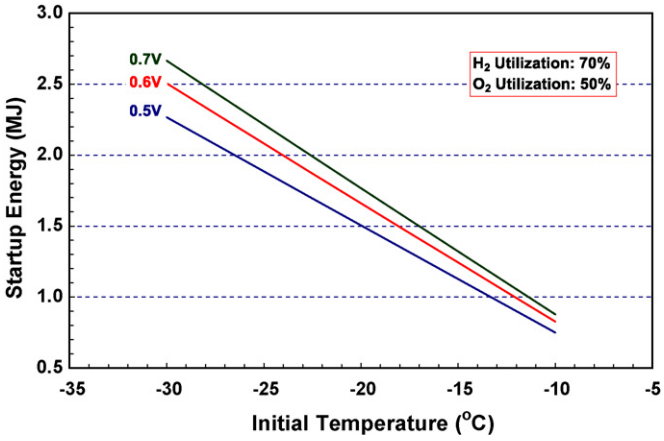

Fig. 9. LHV of hydrogen consumed in warming up the stack to 0 °C from different initial temperatures and cell voltages.

time. Interestingly, a high thermal inertia of the stack impedes its ability to startup from cold temperatures but assists in purging water during shutdown.

4.3. Startup/shutdown energy

We have run simulations to estimate the startup/shutdown energy and expressed it in terms of the lower heating value of fuel hydrogen. We assumed that the electrical energy used to drive the compressor during the purge cycle comes from the energy storage battery that is charged by the stack during the previous drive cycle (50% average fuel cell system efficiency, 85% battery round trip efficiency).

Fig. 9 summarizes the results of simulations for startup energy, i.e., the LHV of hydrogen electrochemically consumed during the time needed to bring the stack to 0 °C. We have not taken any credit for the electrical power generated during the startup time since the power generated in excess of what is needed by the auxiliaries may have to be dissipated if the vehicle is not being driven. As seen in Fig. 9, the startup energy is primarily a function of the ambient temperature and the cell voltage, and it depends only weakly on the initial λ; the startup time, however, is a strong function of λ_i. For example, the startup time is >40 s at −20 °C, V_{cell} = 0.6 V, and λ_i = 4 (see Fig. 5). It can be reduced to <40 s by selecting λ_i = 6, but self-start is not possible at this value of λ_i from −30 °C ambient temperature. The thermal energy needed to raise the stack temperature

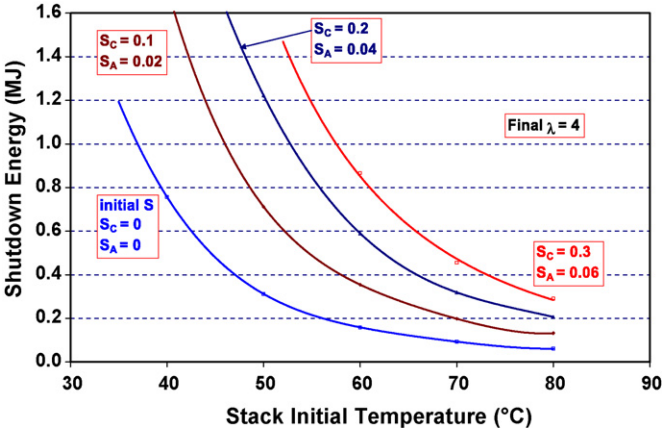

Fig. 10. LHV of hydrogen required to provide the electrical energy consumed by the compressor during shutdown at different initial stack temperatures and saturation levels, target λ = 4.

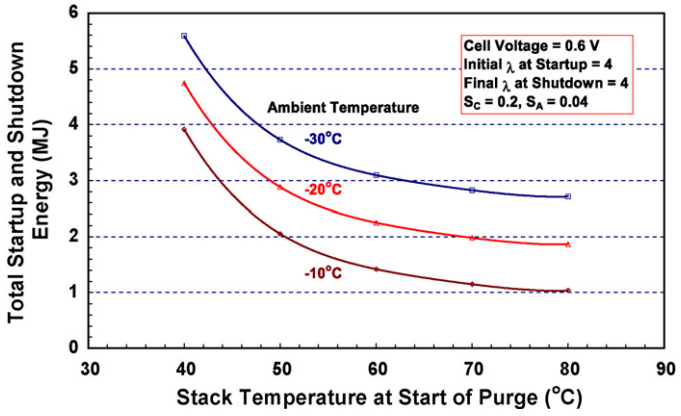

Fig. 11. Total startup and shutdown energy (see legend for initial conditions).

to 0 °C is only a function of the ambient (initial) temperature (fixed stack and coolant heat capacity). This thermal energy is supplied by the waste heat produced in the electrochemical reaction, which is mainly a function of the cell voltage (i.e., electrical inefficiency).

Fig. 10 presents the calculated shutdown energy as a function of the initial stack temperature and GDL saturation for target λ = 4. The shutdown energy was determined by first calculating the electrical energy that the compressor draws from the battery during the shutdown process and then calculating the LHV of hydrogen consumed by the fuel cell system in the previous drive cycle to generate this electrical energy and store it in the battery. Fig. 10 shows that the shutdown energy is quite sensitive to the GDL saturation levels, especially at low initial stack temperatures. Similarly, the shutdown energy depends on the initial stack temperature and increases rapidly as the initial temperature approaches the minimum temperature for which the target λ is achievable.

Finally, Fig. 11 presents the calculated total startup and shutdown energy as a function of the ambient temperature and the stack temperature at start of purge for one value of GDL saturation and target λ (final λ at the end of purge which is the same as initial λ at startup). For the conditions of these simulations, the total energy can be greater than 5 MJ if the ambient temperature is below −20 °C and the stack temperature at the previous shutdown is <40 °C.

5. Summary and conclusions

A dynamic model for water uptake and transport in the membrane and ionomer in the catalyst layers has been used to analyze startup from subfreezing temperatures and stack shutdown for the next subfreezing start. We find that the initial membrane water content is an important parameter that determines whether a successful self-start is possible. There is a critical λ, above which self-start is not possible because the product water completely engulfs the catalyst layers with ice before the stack can warm-up to 0 °C. There is a second value of λ, below which the stack can be self-started without forming ice. Between λ_l and λ_h, the stack can be self-started, but with intermediate formation of ice that melts as the stack warms up to 0 °C. Both λ_l and λ_h are functions of the initial stack temperature, cell voltage at startup, membrane thickness, catalyst loading, and stack heat capacity.

We have also analyzed the time required and the energy consumed during shutdown in order to prepare the stack for a subsequent startup from subfreezing temperatures. We have run simulations to study the drying of the membrane by purging the cathode with air (no anode purge) as a function of the initial stack temperature and water content of the catalyst and gas diffusion layers (saturation levels). We find that, depending on the initial saturation level, it may not be possible to dry the membrane to the

target λ if the stack at the start of the purge cycle is below a certain temperature.

Finally, we have determined the optimum λ for robust and rapid startup and shutdown. Startup and shutdown time and energy may be unacceptable if the λ is much less than the optimum. Conversely, a robust startup from subfreezing temperatures cannot be assured if the λ is much higher than this optimum.

Acknowledgements

This work was supported by the U.S. Department of Energy, Office of Energy Efficiency and Renewable Energy, Fuel Cell Technologies Program. Dr. Nancy Garland and Mr. Jason Marcinkoski were the Technology Development Managers for this study. The authors thank Dr. Romesh Kumar of Argonne National Laboratory for many useful discussions and helpful suggestions. Argonne National Laboratory, a U.S. Department of Energy Office of Science laboratory, is operated by UChicago Argonne, LLC, under Contract No. DE-AC02-06CH11357.

References

[1] Hydrogen, Fuel Cells, and Infrastructure Technologies Program: Multi-Year Research, Development and Demonstration Plan, http://www1.eere.energy.gov/hydrogenandfuelcells/mypp, 2009.
[2] R.K. Ahluwalia, X. Wang, J. Power Sources 162 (2006) 502–512.
[3] Y. Hishinuma, T. Chikahisa, F. Kagami, T. Ogawa, JSME Int. J. Ser. B 47 (2004) 235–241.
[4] M. Oszipok, M. Zedda, D. Riemann, D. Greckeler, J. Power Sources 154 (2006) 404–411.
[5] K. Tajiri, Y. Tabuchi, F. Kagami, S. Takahashi, K. Yoshizawa, C.-Y. Wang, J. Power Sources 165 (2007) 279–286.
[6] S. Ge, C.-Y. Wang, Elecrochem. Solid-State Lett. 9 (2007) A499–A503.
[7] S. Ge, C.-Y. Wang, Electrochim. Acta 52 (2007) 4825–4835.
[8] E. Pinton, Y. Fourneron, S. Rosini, L. Antoni, J. Power Sources 186 (2009) 80–88.
[9] A. Conti, 2009 DOE Hydrogen Program Review, Arlington, VA, May 18–22, 2009.
[10] R. Darling, PEMFC Freeze Technical Workshop, Nuvera Fuel Cells, Billerica, MA, February 20, 2009.
[11] J.P. Owejan, J.J. Gagliardo, T.A. Trabold, Nuvera Fuel Cells, Billerica, MA, February 20, 2009.
[12] J. Li, S. Lee, J. Roberts, Electrochim. Acta 53 (2008) 5391–5396.
[13] K. Jiao, X. Li, Electrochim. Acta 54 (2009) 6876–6891.
[14] F. Jiang, W. Fang, C.-Y. Wang, Electrochim. Acta 53 (2007) 610–621.
[15] P. Sinha, C.-Y. Wang, J. Electrochem. Soc. 154 (2007) B1158–B1166.
[16] K. Tajiri, C.-Y. Wang, Y. Tabuchi, Electrochim. Acta 53 (2008) 6337–6343.
[17] J.P. Owejan, J.J. Gagliardo, S.R. Falta, T.A. Trabold, J. Electrochem. Soc. 156 (2009) B1475–B1483.
[18] E.F. Thompson, T.W. Capehart, T.F. Fuller, J. Jorne, J. Electrochem. Soc. 153 (2006) A2351–A2362.
[19] E.F. Thompson, J. Jorne, H.A. Gasteiger, J. Electrochem. Soc. 154 (2007) B783–B792.
[20] E.F. Thompson, J. Jorne, W. Hu, H.A. Gasteiger, J. Electrochem. Soc. 155 (2008) B625–B634.
[21] E.F. Thompson, J. Jorne, W. Hu, H.A. Gasteiger, J. Electrochem. Soc. 155 (2008) B887–B896.
[22] K.G. Gallagher, B.S. Pivovar, T.F. Fuller, J. Electrochem. Soc. 156 (2009) B330–B338.
[23] H. Yoshida, Y. Miura, J. Membr. Sci. 68 (1992) 1–10.